Innovative Infrastructure Solutions (2026) 11:241
https://doi.org/10.1007/s41062-026-02618-w

TECHNICAL PAPER

Environmental, structural, and economic investigation of 3D-printed concrete buildings with varying cross-sectional geometries

İffet Gamze Mütevelli Özkan[1,2] · Alper Aldemir[3]

Received: 10 March 2025 / Accepted: 13 March 2026 / Published online: 16 April 2026

Abstract

The construction industry is moving towards Industry 4.0, integrating 3D printing into practice. However, existing research often treats structural, environmental, and economic aspects in isolation, lacking a holistic evaluation of building-scale performance under seismic demands. This study addresses this gap by comparing two building-scale 3D printed concrete (3DPC) designs with five types of wall section geometries (filled, carved, square, rectangular, and triangular) in terms of environmental, structural, and economic considerations. The study proposes a holistic preliminary design option and evaluation methodology for 3DPC wall systems in seismic zones. The examined section geometries were selected to reflect commonly adopted practical design approaches, aiming to systematically investigate the trade-offs between load-bearing capacity and material efficiency, ranging from completely filled systems to more material-efficient configurations. The buildings are two-story, and their wall thicknesses are 150 mm and 300 mm. Initially, shear walls were considered as conventional reinforced concrete members. The demanded axial loads for shear walls were calculated for an area of high earthquake risk and compared with the ultimate axial loads of 3DPC walls based on the cross-sectional geometry. In conclusion, for the studied high seismic hazard case, considering axial safety, environmental compatibility, and economic performance, the carved type is the most favorable wall configuration for a 150 mm thickness. For a 300 mm thickness, the most favorable wall configuration depends on the architectural plan.

✉ İffet Gamze Mütevelli Özkan
gamzemutevelli@hacettepe.edu.tr;
gmutevelli@kastamonu.edu.tr

Alper Aldemir
alperaldemir@hacettepe.edu.tr

1 Department of Civil Engineering, Graduate School of Science and Engineering, Hacettepe University, Ankara 06800, Turkey

2 Department of Civil Engineering, Kastamonu University, Kastamonu 37150, Turkey

3 Department of Civil Engineering, Hacettepe University, Ankara 06800, Turkey

Graphical abstract

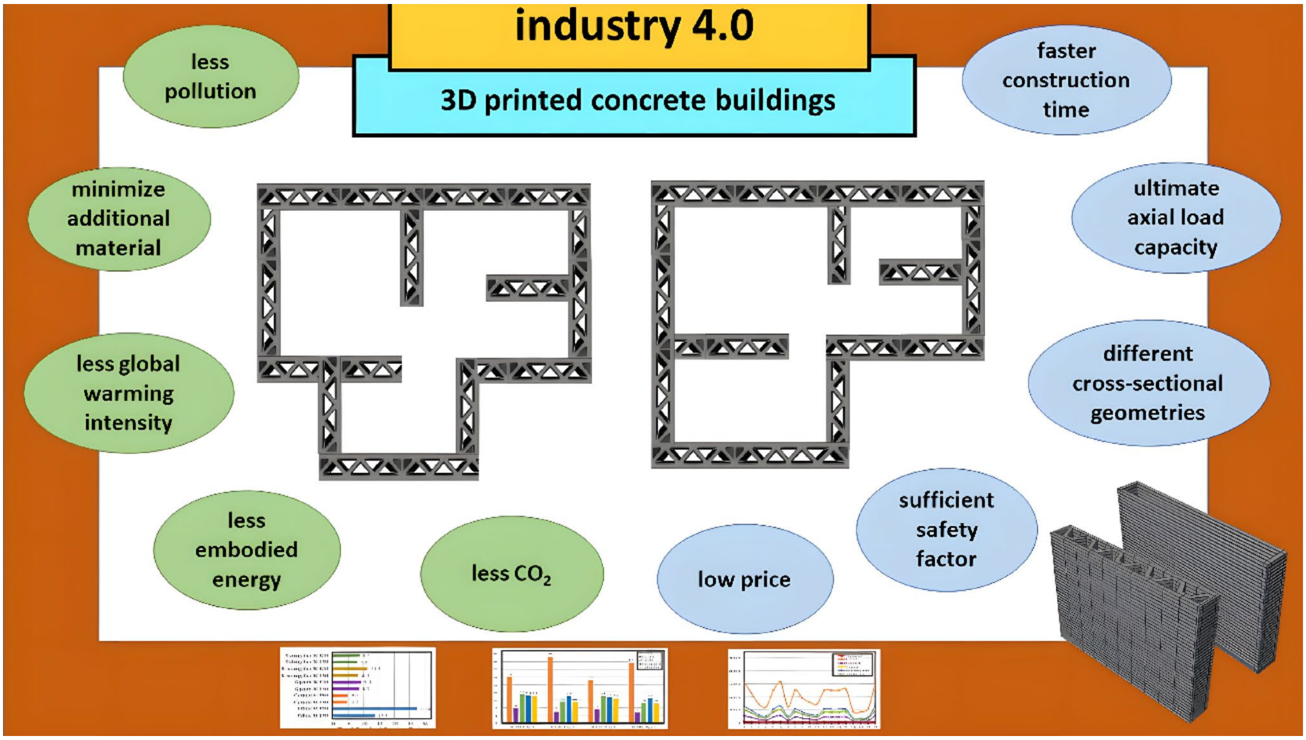

Keywords 3D printed concrete building · Ultimate axial load · Cross-sectional geometry · Environmental compatibility · Industry 4.0

Introduction

The construction industry has lagged in introducing new technologies and has never experienced significant, disruptive change, in contrast to industries such as aerospace or automotive, which have adopted digital innovations to improve quality and efficiency, making radical process changes [1]. However, these pictures have changed in recent years due to the transition to Industry 4.0, and additive manufacturing, also called 3D printing, has emerged as one of the most favorable construction methodologies [2]. The technologies that fall under Industry 4.0 include materials science, artificial intelligence (AI), robots, and printing with 3D printers [3, 4].

A particular printer is required to produce complicated 3D structures from concrete using 3D printing (3DP) technology. The technology puts forward a wide range of potential ecological advantages compared to conventional construction techniques. As a possible alternative to current construction methods, 3D printing is being evaluated for reduced costs, energy efficiency, automation of construction processes, and environmental impact mitigation [5, 6]. To minimize the total amount of concrete required for a planned building, 3D printed concrete (3DPC) technology enables the precise positioning of materials. Thus, resources are protected, and the damage caused by construction to the environment can be minimized. In addition, 3DPC can reduce waste by enabling the production of structures, upon request, of the exact size and shape required without the need for additional material [7, 8]. Muñoz et al. [9] noticed that 3DP technology may be more beneficial to the environment than mass manufacturing for unique things, while mold reuse in traditional methods is less beneficial. It was first started for architectural aesthetics because of its flexibility to create novel geometry and design, and it has since been promoted for cost reduction and material optimization-derived environmental benefits [10–12].

Structural design optimization reportedly reduces costs and carbon emissions for concrete structures by 18–24% [13]. This means that the increased automation potential and greater freedom in production made possible by digital printing technologies can further lower costs and greenhouse gas emissions [14]. The “Apis Cor House” in Russia and the “Office of the Future” in Dubai are examples of 3D-printed structures. The “Office of the Future” is intended to serve the National Committee of the United Arab Emirates (UAE). It is equipped with air conditioning, water, electricity, and telecommunications and serves as a place for group meetings. Thanks to 3DPC, construction waste has been reduced by 30 to 60%, while labor costs have been cut by 50 to 80% [15, 16]. Likewise, the production times have been decreased by 50 to 70% [17, 18].

Portland cement (PC) is the binder used in concrete, which is the most widely used construction material in structures worldwide [19, 20], and it is associated with significant emissions of CO_2 [19–21]. The construction industry is responsible for 40% of global resource consumption and waste production and 33% of greenhouse gas emissions [22, 23]. This situation necessitates a comprehensive evaluation of the environmental impacts of building materials and construction methods, encompassing not only the production phase but also their entire life cycle. Life Cycle Assessment (LCA) serves as a critical methodology for quantifying a product or service's environmental footprint throughout its lifespan. Early application of LCA protocols helps identify environmental hotspot sand potential challenges, thereby aiding in more informed and sustainable decision-making [24, 25]. In the context of emerging construction techniques, LCA contributes significantly to sustainable development in emerging technologies like 3DCP by revealing process-related environmental impacts [26]. Notably, recent LCA-based studies confirm that 3DPC offers substantial environmental and economic benefits, particularly, in large-scale projects. For instance, Weng et al. [27] demonstrated that 3DCP technology offers significant reductions of 25.4% in cost, 85.9% in CO_2 emissions, and 87.1% in energy consumption compared to traditional construction [27, 28]. Mohammad et al. [29] reported that 3DCP assessed via LCA exhibits lower environmental impacts than conventional construction, particularly regarding fossil fuel consumption, global warming potential, acidification, smog, and eutrophication. Overall, 3DCP enables faster, more environmentally friendly, and potentially more cost-effective construction [30].

In addition, the high design freedom offered by additive manufacturing allows material use to be minimized. Moreover, 3DPC facilitates the production of lightweight structures through topology optimization. Structural weight can be further reduced, and thermal insulation can be improved by developing mixtures with materials with low heat conductivity [31, 32]. The outer walls significantly contribute to heat loss, accounting for up to 25% of the total thermal energy loss [32]. Air voids or filling materials, changes in thickness, and cross-sectional forms are among the techniques suggested to control the thermal performance of 3DPC walls [33]. Although it offers environmental and construction benefits, 3DPC presents certain notable limitations. The performance of 3D-printed concrete is primarily influenced by material properties, particularly the interlayer bonding characteristics, which introduce uncertainties regarding mechanical performance and durability [34]. In addition, substantial initial investment costs, complex equipment requirements, and the need for skilled operators are major factors limiting the widespread use of the technology [35–37].

Furthermore, challenges related to maintaining consistent quality and the limited variety of design strategies for secure load transfer pose substantial obstacles to the engineering implementation of this technology [38–42]. As a consequence of these limitations, the load-bearing capacity of the walls in existing buildings and the degree to which the 3D printing technique was integrated into the structures remain unknown [43]. Studies on this topic are underway. In this context, Han et al. [44] determined the axial load capacity of large 3DPC walls, and other researchers have also studied this topic [45–47]. In this case, Mütevelli Özkan and Aldemir [48] used machine learning (ML) algorithms to figure out the ultimate axial load capacities of 3DPC walls with various cross-sectional geometries. In addition, Ozalp and Aldemir presented artificial intelligence (AI) based automated tool to estimate and design 3D printed concrete walls. Therefore, the tools required to automatically design and print the 3D printed concrete buildings started to become available in the literature.

This study aims to investigate the environmental, structural, and economic consequences of constructing buildings using 3D printing technology, specifically focusing on several types of 3DPC walls. Therefore, two buildings with different architectural plans were modeled, and a response spectrum analysis (RSA) was performed to design these structures located in a region with a high earthquake hazard level using SAP2000 [49]. Afterwards, considering five different cross-sectional geometries, ultimate (Ulti.) axial load capacities of the 3DPC walls in the buildings were estimated. The ultimate and demanded (Demand.) axial loads were compared by considering different cross-sectional geometries. Then, considering the wall thicknesses of 150 mm and 300 mm, the amount of material required to print these buildings, their environmental impact, printing times, and prices were compared.

Methodology

Traditional methods in construction industry has some drawbacks in terms of economic reasons, environmental impacts and the quality assurance and quality inspection (QA/QC) of the project. In addition, conventional methods cause material waste and lead to uncontrolled consumption of natural resources. On the other hand, thanks to 3D printing technology, less material waste, less cost, and faster

Table 1 Structural and site conditions of the buildings

Category	Parameter	Assumptions
Material properties	Concrete class	C25
	Rebar class	S420
Story dimensions	1st story height (cm)	400
	2nd story height (cm)	320
Site parameters	Soil class	ZC
	Peak ground acceleration, PGA (g)	0.705
	Peak ground velocity, PGV (cm/s)	55.842
Site coordinates	Latitude (°)	40.705975
	Longitude (°)	29.820707

construction are possible. As sustainability increases, mistakes caused by workers could be eliminated, and the use of molds in the traditional method could be ended. Mainly thanks to rapid construction, the accommodation needs of the victims could be provided urgently after natural disasters. Similarly, in case of an emergency like a pandemic, hospitals could be built quickly as well.

Analysis of buildings

Initially, two different architectural plans were designed, consisting only of shear walls as the vertical structural components. Then, each structure was analyzed using an RSA according to the Turkish Building Earthquake Code (TBEC 2018) [50], which estimates peak structural demands based on the design spectrum. TBEC 2018 is the latest seismic design code in Turkiye and combines the national seismic hazard map with a location-specific design spectrum, enabling seismic demand to be characterized consistently for design purposes. Wall thicknesses of 150 mm and 300 mm were chosen to represent the thin and thick wall options commonly used in 3DPC applications and to comparatively investigate the effect of wall thickness on the load-bearing system. Thicknesses below this range can increase buildability flaws and stability problems, while increasing thickness beyond this range reduces printing efficiency, limiting the comparative value of geometry-based evaluation. The buildings were assumed to be located in the Golcuk region, which has a high seismic risk level [51–53], to more rigorously assess the behavior of different cross-section geometries and wall thicknesses under a demanding seismic scenario. Table 1 summarizes both physical properties of the buildings and the geographical coordinates of the selected building site.

The plan-1 and the plan-2 are shown in Fig. 1, and all dimensions are given in centimeters. The floor areas of plan-1 and plan-2 are 145 m^2, and 135 m^2, respectively. Plan-1 has 18 shear walls, whereas plan-2 has 19 shear walls. The analysis was repeated for plan-1 and plan-2 using 150 mm and 300 mm wall thickness considering two stories (Fig. 2).

The axial force demands were calculated for each shear wall using SAP2000 [49]. Each value was obtained using the load combinations defined in Requirements for Design and Construction of Reinforced Concrete Structures (TS 500) [54] and TBEC 2018 [50].

3D printed concrete walls

A concrete compressive strength of 25 MPa (C25) was selected for the 3DPC walls, representing a commonly reported strength class in the literature for structural evaluation [8, 55–57]. The numerical analysis assumes that the

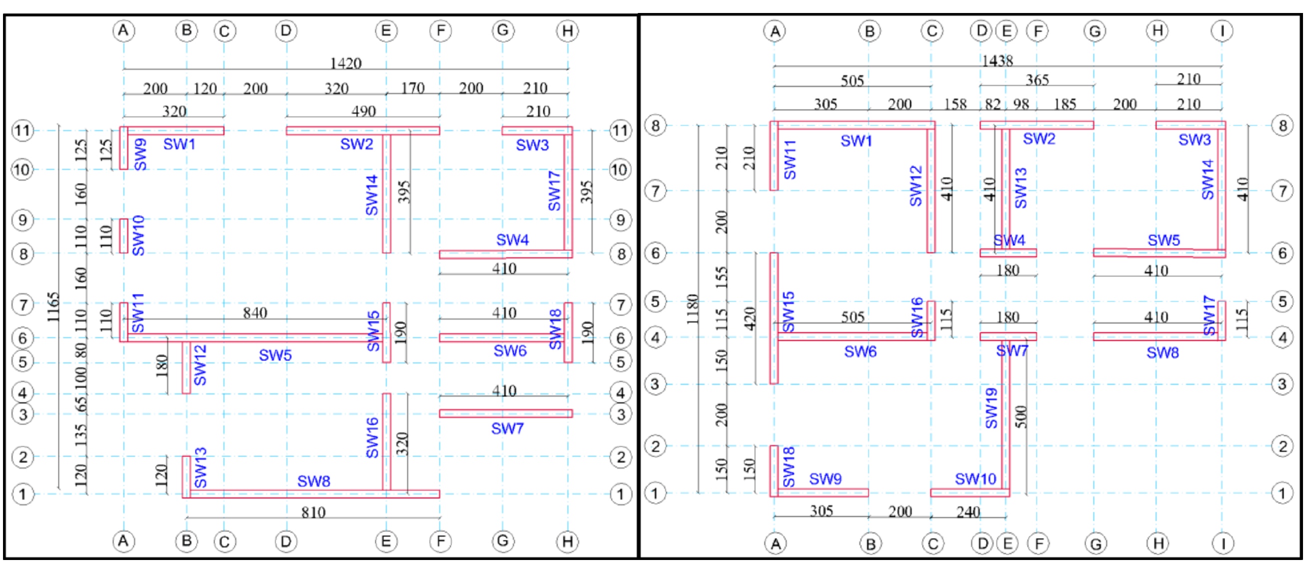

Fig. 1 Architectural plans. **a** plan-1, **b** plan-2

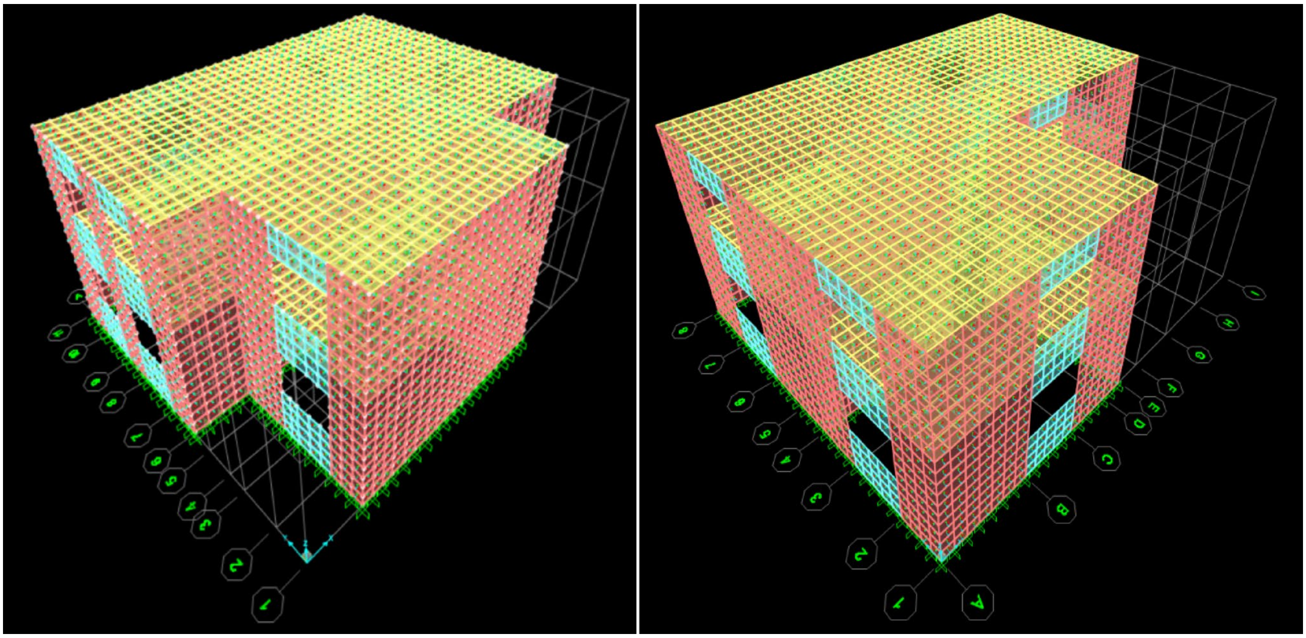

Fig. 2 Numerical models. **a** building-1, **b** building-2

Table 2 Constituents and proportions of mixture for C25

Constituents	Proportions (kg/m^3)
Portland cement (PC)	625
Normal aggregate (NA) - quartz sand	1250
Water	300

Table 3 Life cycle inventory data of utilized materials

Materials	Global warming intensity (kgCO$_2$-eq/t)	Embodied energy (MJ/t)	References
Portland cement	1000	5500	[64, 65]
Normal aggregate	6.20	120	[65, 66]
Water	[a]Not considered	[a]Not considered	[65, 67]

[a]The environmental impacts of water were omitted due to their minimal contribution to the overall global warming potential of concrete production

walls are successfully manufactured with sufficient interlayer bonding, allowing the study to isolate and quantify the effects of cross-sectional geometry. Consequently, the primary objective is to compare the building-scale structural performance of 3DPC wall cross-sectional geometries, the experimental evaluation of fresh state rheological properties (e.g., printability, buildability) and interlayer bonding characteristics was considered beyond the scope of this study. The mix proportions of the C25 3D-printable concrete were defined based on relevant literature, notably the research conducted by Khan et al. [8], as reported in Table 2, to provide the necessary material inventory for the environmental impact analysis.

To create 3DPC walls, the characteristics of the 3D printing robot used in the study of Alhumayani et al. [58] were considered. The robot performs 3D printing processes and carries a load of around 30 kg. It is equipped with six motors on its each axis, and the total power of the motors at maximum capacity is 16.8 kW. 3D printing speed and the perimeter length of the design path line for the walls, including all layers, are necessary to calculate the time needed to complete 3D printing of each building. The speed of the 3D printing was accepted as 0.25 m/s. The robot's operating time to complete 3D printed buildings was calculated by dividing the perimeter of the walls by the 3D printing speed. The perimeter line in 3D printing was the whole length of all layers in the wall system multiplied by the total amount of layers. Additionally, the height of the printing layer in 3DPC walls was accepted as 10 mm. In this study, the mathematical method of estimating electricity consumption in kilowatt-hours (kWh) was preferred. It was calculated by multiplying power demand in kW by the printing time in hours [58].

The issue's importance for the environment becomes clear when concrete includes PC. Therefore, using as much concrete in buildings as is ecologically and economically necessary is essential. Moreover, one ton of PC necessitates the utilization of an estimated 1.5 tonnes of raw materials [59–61]. Table 3 shows the life cycle inventories of the materials utilized in the current study. For 3DPC, $250 per cubic meter was accepted [62, 63], and the volume of concrete in both buildings was multiplied by the price per cubic meter and divided by the two-story buildings' total square meters to calculate the price per square meter.

Mütevelli Özkan and Aldemir [48] proposed 3DPC walls with five different cross-sectional geometries, as shown in Fig. 3. They calculated their ultimate axial load capacity by explicit dynamic analysis using finite element (FE) methods. Then, they used several ML models to train the outputs to predict the ultimate axial load capacity. The ML algorithms provided reliable predictions with a coefficient of determination greater than 0.95 [48]. The ML algorithms used in the study are Random Forest Regressor (RFR), Extra Trees Regressor (ETR), Gradient Boosting Regressor (GBR), Hist Gradient Boosting (HGB), Light Gradient Boosting Machine (LightGBM), and Extreme Gradient Boosting (XGBoost). Then, they also used the average prediction, which calculates the arithmetic mean score of the predicted values.

This study evaluated 150 mm and 300 mm wall thicknesses for the filled, carved, square, rectangular, and triangular types (Fig. 3). The average prediction [48] was used to calculate the building walls' maximum axial load capacity. Then, the safety factor (SF) values were found by dividing the ultimate axial load capacities of the 3DPC wall by the axial load demands calculated in SAP2000 [49].

In this study, the evaluation is limited to the ultimate axial load-carrying capacity and the resulting SF, representing the compressive load-bearing safety of walls. Axial load demands obtained from RSA performed for a high-seismic hazard zone provide a fundamental criterion for the preliminary evaluation of the structural safety of load-bearing walls. Ensuring sufficient axial load-carrying capacity is a prerequisite for a meaningful evaluation of shear and bending behaviors. Therefore, the presented results should not be interpreted as a final seismic performance evaluation; rather, they constitute a preliminary design and pre-selection methodology that allows for the comparison of different cross-sectional geometries in terms of axial load-bearing safety.

Results and discussion

The study compared the ultimate and demanded axial loads of walls with five different cross-sectional geometries for two different architectural plans. The comparison also evaluated the effect of different wall thicknesses (i.e., 150 mm and 300 mm) for each plan. In addition, the quantity of material needed to print these structures, their environmental impact, printing durations, and costs were also assessed.

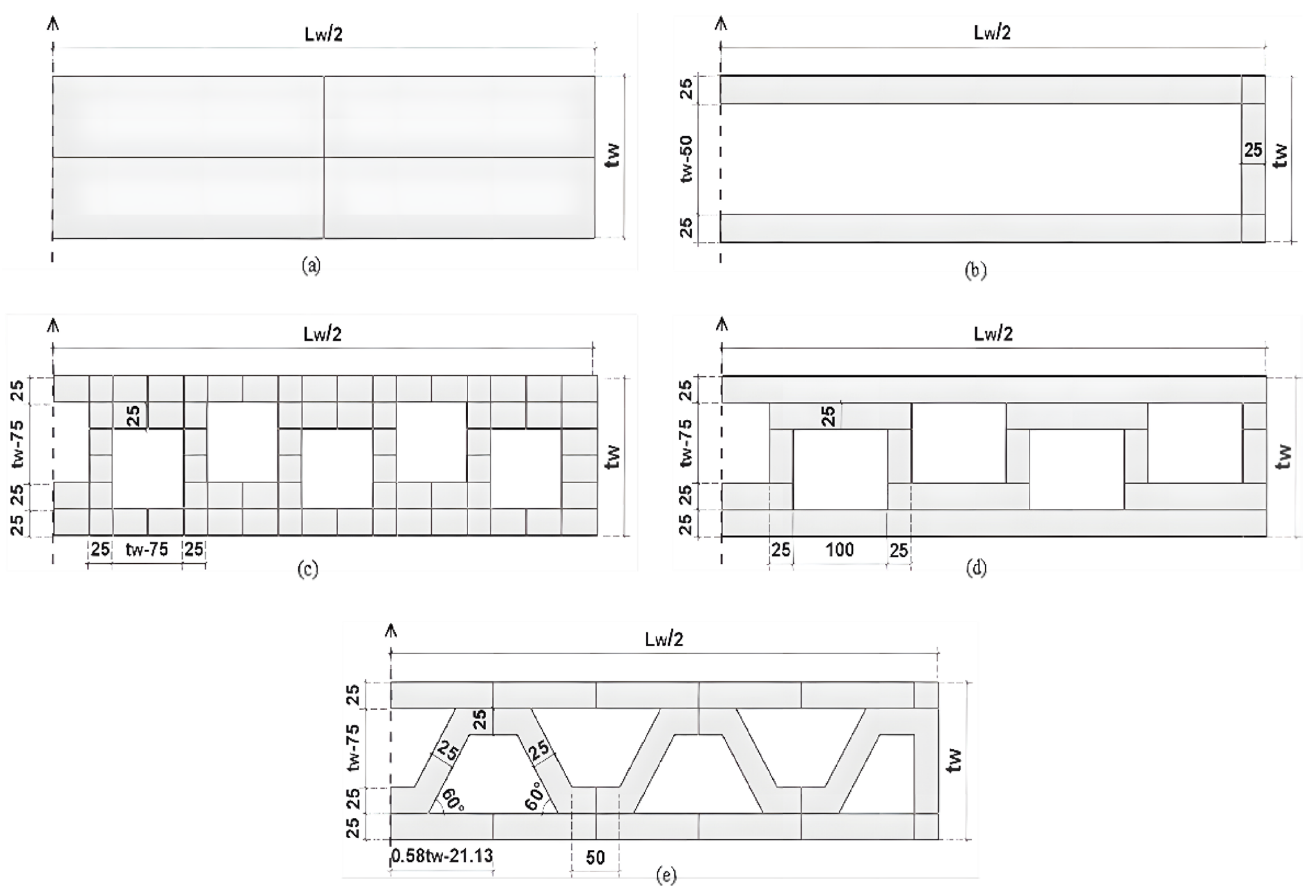

Fig. 3 Symmetric cross-section dimensions of 3DPC wall types. **a** filled type, **b** carved type, **c** square type, **d** rectangular type, **e** triangular type [48]

Table 4 The case of 150 mm wall thicknesses for 3DPC wall types in plan-1

Wall type	Filled	Carved	Square	Rectangular	Triangular
Concrete volume (m^3)	74.3	25.6	46.9	45.0	42.6
Void volume (m^3)	0.0	48.7	27.4	29.2	31.6
Void volume to concrete volume ratio	0.0	1.9	0.6	0.6	0.7
Concrete fulled mass (t)	178.2	61.3	112.5	108.1	102.3
Savings of concrete according to the filled type	0.0%	65.6%	36.9%	39.3%	42.6%
Completed duration (Day)	13.8	4.7	8.7	8.3	7.9
Price ($/$m^2$)	64.0	22.0	40.4	38.8	36.8
Electricity consumption (kWh)	5544.9	1908.6	3499.5	3363.1	3183.1
Electricity consumption ratio according to the filled type	100.0%	34.4%	63.1%	60.7%	57.4%
PC consumption (t)	46.4	16.0	29.3	28.2	26.6
Water consumption (t)	22.3	7.7	14.1	13.5	12.8
NA consumption (t)	92.8	32.0	58.6	56.3	53.3
Raw material consumption (t)	69.6	24.0	43.9	42.2	40.0
Global warming intensity of PC ($kgCO_2$-eq)	46413.8	15976.3	29292.7	28151.3	26644.0
Embodied energy of PC (MJ)	255275.6	87869.4	161109.6	154831.9	146542.1
Global warming intensity of NA ($kgCO_2$-eq)	575.5	198.1	363.2	349.1	330.4
Embodied energy of NA (MJ)	11139.3	3834.3	7030.2	6756.3	6394.6

Table 5 The case of 300 mm wall thicknesses for 3DPC wall types in plan-1

Wall type	Filled	Carved	Square	Rectangular	Triangular
Concrete volume (m^3)	148.5	26.8	49.9	60.9	47.1
Void volume (m^3)	0.0	121.8	98.6	87.7	101.4
Void volume to concrete volume ratio	0.0	4.5	2.0	1.4	2.2
Concrete fulled mass (t)	356.5	64.3	119.8	146.1	113.0
Savings of concrete according to the filled type	0.0%	82.0%	66.4%	59.0%	68.3%
Completed duration (Day)	27.5	5.0	9.2	11.3	8.7
Price ($/$m^2$)	128.1	23.1	43.0	52.5	40.6
Electricity consumption (kWh)	11089.8	1999.1	3726.4	4544.5	3515.9
Electricity consumption ratio according to the filled type	100.0%	18.0%	33.6%	41.0%	31.7%
PC consumption (t)	92.8	16.7	31.2	38.0	29.4
Water consumption (t)	44.6	8.0	15.0	18.3	14.1
NA consumption (t)	185.7	33.5	62.4	76.1	58.9
Raw material consumption (t)	139.2	25.1	46.8	57.1	44.1
Global warming intensity of PC ($kgCO_2$-eq)	92827.5	16733.8	31191.6	38040.0	29429.6
Embodied energy of PC (MJ)	510551.3	92035.6	171553.6	209220.0	161862.6
Global warming intensity of NA ($kgCO_2$-eq)	1151.1	207.5	386.8	471.7	364.9
Embodied energy of NA (MJ)	22278.6	4016.1	7486.0	9129.6	7063.1

In this context, W150 denotes a building with 150-mm-thick walls, and W300 represents a building with 300-mm-thick walls.

Comparison of 3DPC buildings from an ecological and economic point of view

The material quantities used for each wall type belonging to W150 in plan-1 are shown in Table 4. Similarly, Table 5 lists the quantities of materials used for each wall type in the W300 configuration in plan-1. In addition, Table 6 gives the quantities of materials used for each wall type in plan-2 belonging to W150, while Table 7 gives them for each wall type in the W300 in plan-2.

Material saving rates were calculated separately for each wall type by using the filled type wall model with the same external dimensions as the reference. Since the cross-sectional geometry remains constant along the wall length, the cross-sectional area of the relevant wall type ($A_{relevant}$) was subtracted from the cross-sectional area of the filled type

Table 6 The case of 150 mm wall thicknesses for 3DPC wall types in plan-2

Wall type	Filled	Carved	Square	Rectangular	Triangular
Concrete volume (m^3)	74.0	25.5	46.7	44.9	42.5
Void volume (m^3)	0.0	48.5	27.3	29.1	31.5
Void volume to concrete volume ratio	0.0	1.9	0.6	0.6	0.7
Concrete fulled mass (t)	177.6	61.2	112.1	107.8	102.0
Savings of concrete according to the filled type	0.0%	65.5%	36.9%	39.3%	42.6%
Completed duration (Day)	13.7	4.7	8.7	8.3	7.9
Price ($/m^2)	68.5	23.6	43.3	41.6	39.3
Electricity consumption (kWh)	5525.9	1904.6	3488.9	3353.1	3173.8
Electricity consumption ratio according to the filled type	100.0%	34.5%	63.1%	60.7%	57.4%
PC consumption (t)	46.3	15.9	29.2	28.1	26.6
Water consumption (t)	22.2	7.7	14.0	13.5	12.8
NA consumption (t)	92.5	31.9	58.4	56.1	53.1
Raw material consumption (t)	69.4	23.9	43.8	42.1	39.8
Global warming intensity of PC (kgCO_2-eq)	46255.1	15942.1	29204.1	28067.3	26566.3
Embodied energy of PC (MJ)	254403.2	87681.7	160622.3	154370.3	146114.4
Global warming intensity of NA (kgCO_2-eq)	573.6	197.7	362.1	348.0	329.4
Embodied energy of NA (MJ)	11101.2	3826.1	7009.0	6736.2	6375.9

Table 7 The case of 300 mm wall thicknesses for 3DPC wall types in plan-2

Wall type	Filled	Carved	Square	Rectangular	Triangular
Concrete volume (m^3)	148.0	26.8	49.8	60.7	47.0
Void volume (m^3)	0.0	121.3	98.2	87.3	101.0
Void volume to concrete volume ratio	0.0	4.5	2.0	1.4	2.1
Concrete fulled mass (t)	355.2	64.2	119.5	145.7	112.8
Savings of concrete according to the filled type	0.0%	81.9%	66.4%	59.0%	68.3%
Completed duration (Day)	27.4	5.0	9.2	11.2	8.7
Price ($/m^2)	137.0	24.8	46.1	56.2	43.5
Electricity consumption (kWh)	11051.9	1998.4	3718.6	4533.4	3508.9
Electricity consumption ratio according to the filled type	100.0%	18.1%	33.6%	41.0%	31.7%
PC consumption (t)	92.5	16.7	31.1	37.9	29.4
Water consumption (t)	44.4	8.0	14.9	18.2	14.1
NA consumption (t)	185.0	33.5	62.3	75.9	58.7
Raw material consumption (t)	138.8	25.1	46.7	56.9	44.1
Global warming intensity of PC (kgCO_2-eq)	92510.3	16727.8	31126.4	37946.9	29371.6
Embodied energy of PC (MJ)	508806.4	92002.6	171195.3	208707.7	161544.0
Global warming intensity of NA (kgCO_2-eq)	1147.1	207.4	386.0	470.5	364.2
Embodied energy of NA (MJ)	22202.5	4014.7	7470.3	9107.2	7049.2

(Afilled) to calculate the concrete saving rate (CSR) for each wall type as defined in Eq. (1).

$$\mathrm{CSR} = \frac{\mathrm{A_{filled}} - \mathrm{A_{relevant}}}{\mathrm{A_{filled}}} \times 100 \quad (1)$$

The nonlinear variation of material saving with wall thickness arises because the hollow cross-sectional geometries are not scaled proportionally as thickness increases. Specifically, since the thickness of the printed elements (shells and trusses) remains constant, increasing the total wall thickness leads to a disproportionate increase in the void area, resulting in higher material efficiency.

In both plans for the W150, the ratio of material saved according to the filled type is 65.6% for the carved type, 42.6% for the triangular type, 39.3% for the rectangular type, and 36.9% for the square type (Tables 4 and 6). In both plans, for the W300 buildings, the percentage of material saved according to the filled type is 82.0% for the carved type, 68.3% for the triangular type, 66.4% for the square

Table 8 The ratio of mass differences between 150 mm wall thickness and 300 mm wall thickness depending on wall type in plan-1 and plan-2

Wall type	Plan-1 concrete fulled mass (t)			Plan-2 concrete fulled mass (t)		
	W150	W300	Differences	W150	W300	Differences
Filled	178.2	356.5	50.0%	177.6	355.2	50.0%
Carved	61.3	64.3	4.5%	61.2	64.2	4.7%
Square	112.5	119.8	6.1%	112.1	119.5	6.2%
Rectangular	108.1	146.1	26.0%	107.8	145.7	26.0%
Triangular	102.3	113.0	9.5%	102.0	112.8	9.6%

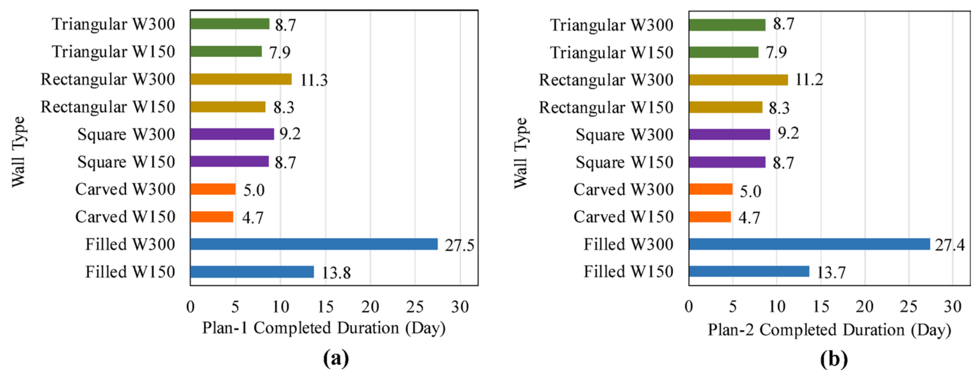

Fig. 4 Completed duration for all 3DPC wall types. **a** for plan-1, **b** for plan-2

type, and 59.0% for the rectangular type (Tables 5 and 7). Accordingly, compared to the filled type, the highest material profit was seen in the carved type for W150 and W300, while the lowest material profit was seen in the square type for W150 and the rectangular type for W300.

When evaluating the void-to-concrete ratio of the cavity walls of the W150, it is determined that the carved type has the highest void ratio at 1.9, followed by the triangular type at 0.7, and finally, the rectangular and square types at 0.6 (Tables 4 and 6). The carved type of the W300 has the highest void ratio at 4.5, followed by the square type at about 2.2, the carved type at 2.0, and the rectangular type at 1.4 (Tables 5 and 7). By filling the cavities in 3DPC walls with thermal insulation material, the thermal insulation performance of the walls can be increased. Thus, wall types with a higher void ratio have better thermal insulation properties. In this context, the thickness of the wall is also important. Considering the wall thicknesses and wall types, it can be seen that the carved type W300 has the highest thermal insulation performance, followed by the triangular type W300. In contrast, the rectangular type W150 and the square type W150 have the lowest thermal insulation performance. In general, the thermal insulation of the W300 is better than that of the W150. However, the rectangular type has the worst thermal insulation among the 300 mm wall types, and it was found that the carved type in W150 has better thermal insulation than the rectangular type in W300, which has even the worst thermal insulation.

Table 8 shows an evaluation of the 3DPC wall types according to their thickness for the two plans. The percentage of material used in W150 is 4.5% to 4.7%, 6.1% to 6.2%, 9.5% to 9.6%, 26.0%, and 50.0% less than in W300 for the carved, square, triangular, rectangular, and filled types, respectively.

Figure 4 shows the completed duration of the W150 and W300 for both plans. The completion time of both W150 is 4.7 days for the carved type, 7.9 days for the triangular type, 8.3 days for the rectangular type, 8.7 days for the square type, and approximately 13.8 days for the filled type. On the other hand, the completion time of both W300 is 5.0 days for the carved type, 8.7 days for the triangular type, 9.2 days for the square type, approximately 11.3 days for the rectangular type, and approximately 27.5 days for the filled type.

When the values are examined, the printing time of the filled wall type of both W150 is approximately 2.9 times that of the carved type, 1.7 times that of the triangular type, and 1.6 times that of the rectangular and square types. The printing time of the filled wall type of both W300 is approximately 5.5 times that of the carved type, 3.2 times that of the triangular type, 3.0 times that of the square type, and 2.4 times that of the rectangular type. It can be seen that all wall types have shorter printing times than the filled type for both the W150 and W300. Especially among wall types with a 300 mm wall thickness, the carved type is completed very quickly and offers considerable time savings. Although the triangular type follows this, the printing times of other wall types are close to each other.

Figure 5 shows the price values of the W150 and W300 for both plans. The price value for the W150 in plan-1 per square meter is 22$ for the carved type, 36.8$ for the triangular type, 38.8$ for the rectangular type, 40.4$ for the square type, and 64.0$ for the filled type. For the W300 in plan-1, the price value per square meter is 23.1$ for the carved type, 40.6$ for the triangular type, 43.0$ for the

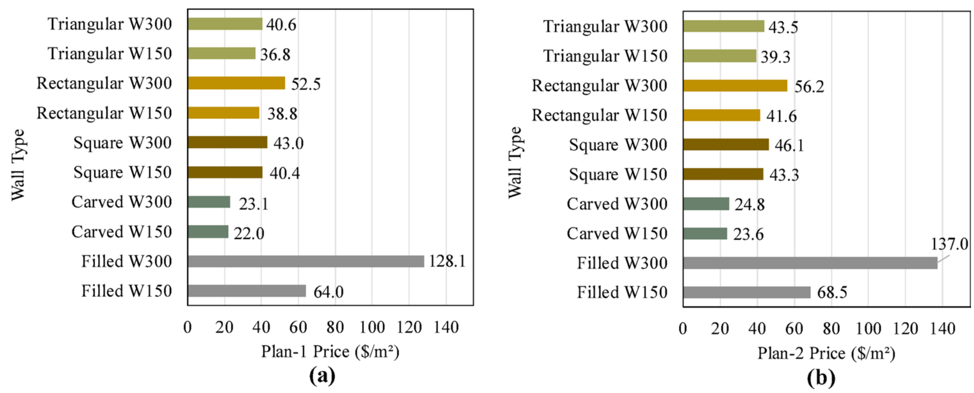

Fig. 5 Concrete cost for all 3DPC wall types. **a** for plan-1, **b** for plan-2

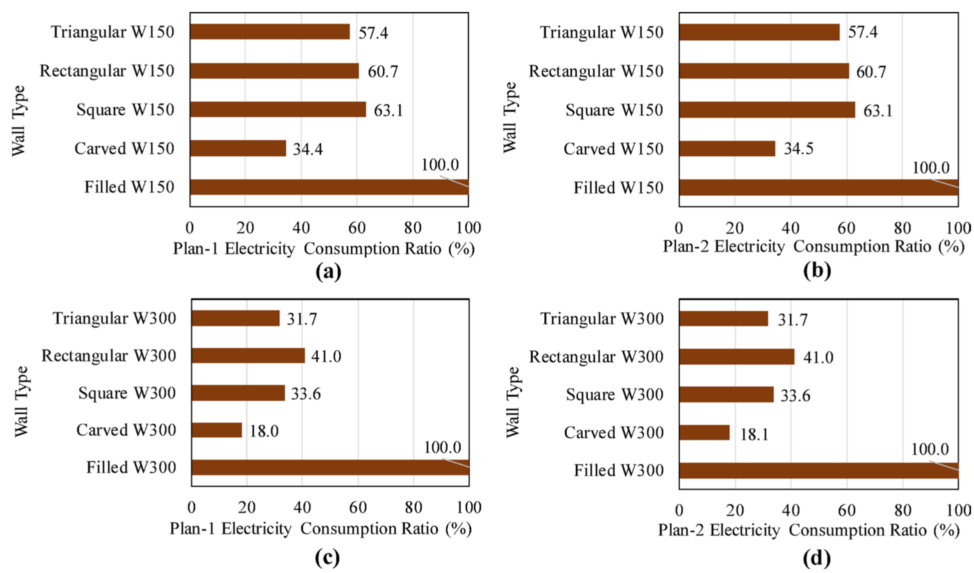

Fig. 6 Electricity consumption percentage based on the filled type. **a** W150 in plan-1, **b** W300 in plan-1, **c** W150 in plan-2, **d** W300 in plan-2

square type, 52.5$ for the rectangular type, and 128.1$ for the filled type. (Fig. 5a). Likewise, the price value for W150 in plan-2 is 23.6$ per square for the carved type, 39.3$ for the triangular type, 41.6$ for the rectangular type, 43.3$ for the square type, and 68.5$ for the filled type. For W300 in plan-2, the price value per square is 24.8$ for the carved type, 43.5$ for the triangular type, 46.1$ for the square type, 56.2$ for the rectangular type, and 137.0$ for the filled type. (Fig. 5b).

When the prices are evaluated, W300 for the filled type has the highest price, while W150 for the carved type has the lowest price. The condition with the highest price is 5.8 times more expensive than the condition with the lowest price. That shows that the W150 for the carved type is much less costly than the W300 for the filled type.

Figure 6 shows the electricity consumption ratio based on the filled type of the W150 and W300 for both plans. In both plans for the W150, the carved type consumes about 34.5% of the electricity consumed by the filled type. The square type consumes 63.1% of the electricity consumed by the filled type, the rectangular type consumes 60.7% of the electricity consumed by the filled type, and the triangular type consumes 57.4% of the electricity consumed by the filled type (Fig. 6a and b). In both plans for the W300 building, the carved type consumes about 18.1% of the electricity the filled type consumes. The square type consumes 33.6% of the electricity consumed by the filled type, the rectangular type consumes 41.0% of the electricity consumed by the filled type, and the triangular type consumes 31.7% of the electricity consumed by the filled type (Fig. 6c and d).

In addition, the consumption values for PC, water, NA, and raw materials for all wall types in plan-1 are listed in Table 4 for W150 and Table 5 for W300. The consumption values for PC, water, NA, and raw materials for all wall types in plan-2 are given in Table 6 for W150 and Table 7 for W300. When the values are discussed, it is understood that the consumption is highest in the filled type and least in the carved type for both W150 and W300 in both plans.

Figure 7 shows the total global warming intensity values, including those for PC and NA. According to the values, for both W150 and W300, the filled type produces the most CO_2 emissions, while the carved type produces the least. Compared to the filled type, the carved type emits 30814.9 $kgCO_2$-eq less in plan-1 for W150, 30688.9 $kgCO_2$-eq less

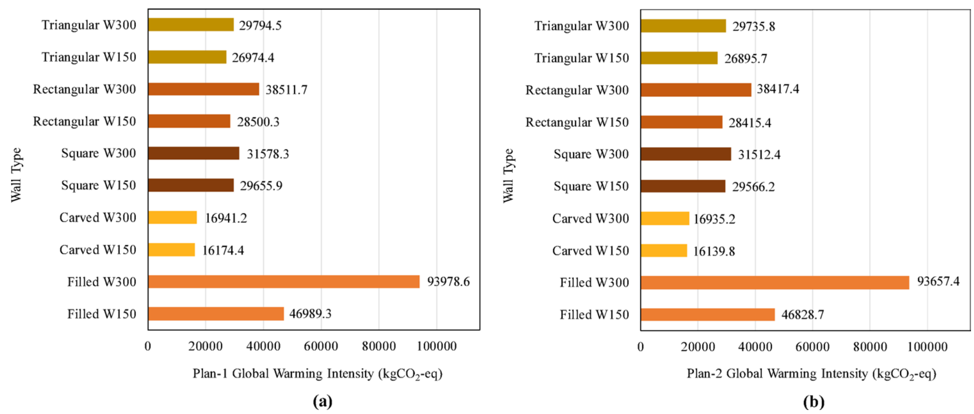

Fig. 7 Total global warming intensity resulting from the usage of PC and NA for all 3DPC wall types. **a** for plan-1, **b** for plan-2

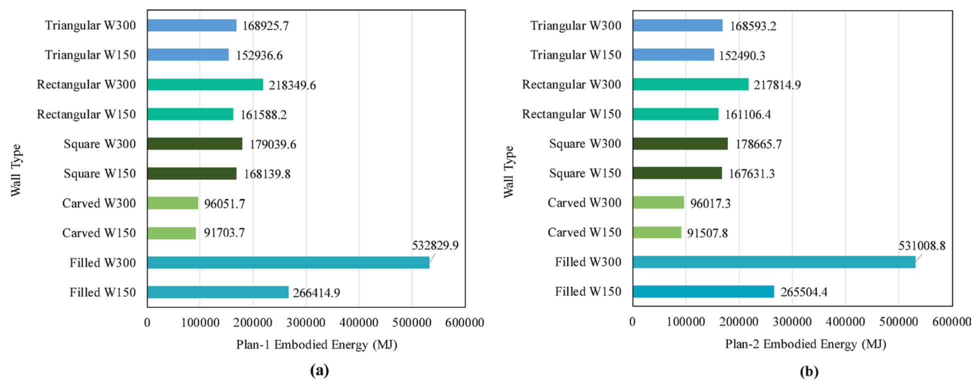

Fig. 8 Total embodied energy resulting from the usage of PC and NA for all 3DPC wall types. **a** for plan-1, **b** for plan-2

in plan-2 for W150, 77037.3 $kgCO_2$-eq less in plan-1 for W300, and 76722.2 $kgCO_2$-eq less in plan-2 for W300.

Figure 8 shows the total embodied energy values that include PC and NA. According to the values, for both W150 and W300, the filled type consumes the most embodied energy, while the carved type consumes the least. Compared to the filled type, the carved type consumes 174711.3 MJ less in plan-1 for W150, 173996.6 MJ less in plan-2 for W150, 436778.1 MJ less in plan-1 for W300, and 434991.6 MJ less in plan-2 for W300.

Comparison of 3DPC buildings from a structural point of view

The demanded axial load, the ultimate axial load capacity, and SF values of each 3DPC wall for W150 and W300 in plan-1 are listed in Tables 9 and 10, respectively. In addition, these values for W150 and W300 in plan-2 are given in Tables 11 and 12, respectively. When the SF values of the printed wall types for W150 in plan-1 are examined, the lowest value is 1.2 in the carved type, while it is approximately 2.0 in the square, rectangular, and triangular types. In plan-2, the lowest value is approximately 7.0 in the carved type, approximately 11.0 in the triangular type, and approximately 12.0 in the rectangular and square types. Additionally, upon examining the SF values of the printed wall types for W300 in plan-1, the lowest value is 0.94 in the carved type, while it is approximately 2.0 in the square, rectangular, and triangular types. In plan-2, the lowest value is approximately 5.0 in the carved type, approximately 9.0 in the triangular and square types, and approximately 11.0 in the rectangular type. In addition, the SF values for the filled walls are larger for W150 and W300 in both plans.

Table 10 shows that the SF = 0.94 value obtained for the W300 carved type indicates that this section geometry does not provide sufficient safety. In high-risk earthquake zones, an SF below 1.0 implies that the structural element lacks adequate capacity to resist the anticipated seismic demands, potentially leading to structural instability or failure. Therefore, this section is not considered an appropriate design option for this thickness; consequently, the wall thickness should be adjusted, or an alternative section geometry should be preferred for safe use.

Upon evaluating the SF distribution, the minimum value among the cases with SF > 1.0 is 1.2. To account for potential uncertainties in ML-based capacity predictions, a conservative sensitivity scenario was considered, assuming a 15% reduction in ultimate axial capacity. Even under this condition, the corresponding SF remains above unity ($0.85 \times 1.2 = 1.02$). This indicates that reasonable levels of prediction uncertainty are unlikely to alter the overall interpretation of axial safety or the comparative trends among the investigated cross-sectional geometries. Accordingly, the SF values are considered not as an absolute design

Table 9 Ultimate axial load values of 150 mm wall thicknesses for 3DPC wall types in plan-1

Wall type			Filled		Carved		Square		Rectangular		Triangular	
No	L_w (mm)	Demand. axial load (kN)	Ulti. axial load (kN)	SF	Ulti. axial load (kN)	SF	Ulti. axial load (kN)	SF	Ulti. axial load (kN)	SF	Ulti. axial load (kN)	SF
1	3200	2672	10200	4	3295	1.2	6255	2	5664	2	5749	2
2	4900	723	15523	21	5069	7	9425	13	9091	13	8564	12
3	2100	393	6925	18	2196	6	4320	11	4137	11	3995	10
4	4100	517	12755	25	4280	8	8030	16	7571	15	7233	14
5	8400	993	26083	26	8526	9	15699	16	15579	16	14190	14
6	4100	480	12755	27	4280	9	8030	17	7571	16	7233	15
7	4100	418	12755	30	4280	10	8030	19	7571	18	7233	17
8	8100	1237	25310	20	8375	7	15273	12	15009	12	13950	11
9	1250	194	4183	22	1343	7	2607	13	2642	14	2505	13
10	1100	75	4016	54	1237	17	2417	32	2413	32	2299	31
11	1100	170	4016	24	1237	7	2417	14	2413	14	2299	14
12	1800	187	5933	32	1887	10	3702	20	3621	19	3506	19
13	1200	186	4171	22	1319	7	2585	14	2476	13	2467	13
14	3950	710	12542	18	4091	6	7659	11	7130	10	7074	10
15	1900	355	6207	18	1948	5	3946	11	3675	10	3653	10
16	3200	477	10200	21	3295	7	6255	13	5664	12	5749	12
17	3950	544	12542	23	4091	8	7659	14	7130	13	7074	13
18	1900	200	6207	31	1948	10	3946	20	3675	18	3653	18
Average		585	10685	24	3483	8	6570	15	6280	14	6024	14

specifications, but as a preliminary screening criterion for evaluating the relative axial load-bearing safety of different wall geometries.

Figure 9 shows the average SF values of all 3DPC wall types in both plans for W150 and W300. In plan-1 for W150, the average SF value was 8.0 for the carved type, 14.0 for the triangular and rectangular types, 15.0 for the square type, and 24.0 for the filled type. In plan-2 for W150, the average SF value was 7.0 for the carved type, 13.0 for the triangular and rectangular types, 14.0 for the square type, and 22.0 for the filled type. It was also found that in plan-1 for W300, the average SF value was 6.0 for the carved type, 11.0 for the triangular and square types, 14.0 for the rectangular type, and 35.0 for the filled type. In plan-2 for W300, the average SF value was 5.0 for the carved type, 10.0 for the triangular and square types, 13.0 for the rectangular type, and 31.0 for the filled type. It can be seen that the lowest average SF belongs to the carved wall types, while the highest average SF belongs to the filled wall types for W150 and W300 in both plans.

It has been observed that the axial load values demanded in a region of high seismicity are lower than the ultimate axial load capacities for 150 mm wall thickness in both plans (Table 9). On the other hand, for 300 mm wall thickness, it was observed that the axial load value demanded on wall 1 for the carved type in plan-1 was greater than the ultimate axial load capacity (Table 10). However, in plan-2, it was determined that the demanded axial load values were lower than the ultimate axial load capacities (Tables 11 and 12). In summary, the lowest maximum axial load values appear for the carved type, and even for this wall type, the demanded axial load values are generally met. The filled type exhibits the greatest ultimate axial load values among all wall types and is significantly greater than the demanded axial load values for the Golcuk region (Fig. 10).

Based on the data obtained, it was determined that the usability of the carved type for a region with a high probability of earthquakes varies depending on the plan shape and wall thickness. Considering the results from capacity, environmental, and economic points of view, it is found that the carved type is most suitable for plan-1 and plan-2, followed by the triangular type, the square type, and the rectangular type for 150 mm wall thickness. For 300 mm wall thickness, it can be seen that the triangular type is the most suitable for plan-1, followed by the square and the rectangular types. For plan-2, the carved type is most suitable, followed by the triangular, square, and rectangular types. The filled type shows very high values for the axial load-bearing capacity for the wall thicknesses of 150 mm and 300 mm for both plans, while it is the last type to be preferred from an ecological and economic point of view.

Conclusions

3D printing technologies have recently gained increasing importance in the construction industry; however, the material consumption, environmental impacts, and load-bearing capacity of 3DPC walls vary significantly depending on their cross-sectional geometry. This study compares the axial demand values of conventional shear walls with thicknesses of 150 mm and 300 mm to the axial load-bearing capacities of 3DPC walls with five different cross-sectional geometries in a high-seismicity region. Additionally, the differences in axial load-bearing capacity, cost, printing duration, resource consumption, and environmental effects of buildings according to wall type are assessed.

The following key results were obtained in the study:

- Regarding material-use efficiency, the carved type offers the highest performance for both W150 and W300, whereas the lowest efficiency is observed in the square type for W150 and the rectangular type for W300.
- W300 consumes more material than W150 in all wall types. The increase in material consumption is greatest in the filled type, followed by rectangular, triangular, square, and carved types.
- Concerning thermal insulation, the W300 carved type offers the highest level of insulation, while the W300 triangular type ranks second. Conversely, the W150 rectangular and square types exhibit the lowest levels of thermal insulation.
- For printing time, the carved type has the shortest duration for both W150 and W300, followed by the triangular type.
- In terms of cost, the W300 filled type has the highest cost, whereas the W150 carved type is the most economical. The highest-priced W300 filled type is 5.8 times more expensive than the lowest-priced W150 carved type.
- Electricity consumption, global warming intensity, and embodied energy are highest in the filled type and lowest in the carved type.
- The applicability of the carved type for a region with high seismic hazard varies depending on the architectural plan and the thickness of the carved walls.
- The filled type provides a capacity far exceeding the demand forces for both architectural plans; however, it results in higher CO_2 emissions due to greater material consumption.
- In a high-seismicity region, considering axial safety, environmental performance, and economic aspects, the W150 carved type is most favorable for plan-1 and plan-2. For W300, the triangular type is most favorable for plan-1, and the carved type is most favorable for plan-2.

Table 10 Ultimate axial load values of 300 mm wall thicknesses for 3DPC wall types in plan-1

Wall type			Filled		Carved		Square		Rectangular		Triangular	
No	L_w (mm)	Demand. axial load (kN)	Ulti. axial load (kN)	SF	Ulti. axial load (kN)	SF	Ulti. axial load (kN)	SF	Ulti. Axial load (kN)	SF	Ulti. axial load (kN)	SF
1	3200	3763	19739	5	3552	0.94	6787	2	8308	2	6630	2
2	4900	1009	30292	30	5314	5	10124	10	12418	12	9707	10
3	2100	559	14487	26	2455	4	4728	8	5847	10	4602	8
4	4100	731	25094	34	4482	6	8614	12	10511	14	8245	11
5	8400	1345	51787	38	8689	6	16951	13	20864	16	15749	12
6	4100	691	25094	36	4482	6	8614	12	10511	15	8245	12
7	4100	651	25094	39	4482	7	8614	13	10511	16	8245	13
8	8100	1774	50569	28	8584	5	16504	9	20526	12	15290	9
9	1250	274	8979	33	1484	5	2825	10	3563	13	2846	10
10	1100	105	8380	80	1380	13	2611	25	3218	31	2720	26
11	1100	241	8380	35	1380	6	2611	11	3218	13	2720	11
12	1800	266	12324	46	2088	8	3997	15	5028	19	4019	15
13	1200	266	8702	33	1434	5	2771	10	3371	13	2812	11
14	3950	944	24245	26	4313	5	8312	9	10062	11	8012	8
15	1900	487	13226	27	2193	4	4274	9	5246	11	4214	9
16	3200	677	19739	29	3552	5	6787	10	8308	12	6630	10
17	3950	793	24245	31	4313	5	8312	10	10062	13	8012	10
18	1900	291	13226	45	2193	8	4274	15	5246	18	4214	14
Average		826	21311	35	3687	6	7095	11	8712	14	6828	11

Table 11 Ultimate axial load values of 150 mm wall thicknesses for 3DPC wall types in plan-2

Wall type			Filled		Carved		Square		Rectangular		Triangular	
No	L_w (mm)	Demand. axial load (kN)	Ulti. axial load (kN)	SF	Ulti. axial load (kN)	SF	Ulti. axial load (kN)	SF	Ulti. axial load (kN)	SF	Ulti. axial load (kN)	SF
1	5050	779	15997	21	5277	7	9727	12	9383	12	8795	11
2	3650	454	11612	26	3806	8	7157	16	6836	15	6547	14
3	2100	328	6925	21	2196	7	4320	13	4137	13	3995	12
4	1800	388	5933	15	1887	5	3702	10	3621	9	3506	9
5	4100	573	12755	22	4280	7	8030	14	7571	13	7233	13
6	5050	674	15997	24	5277	8	9727	14	9383	14	8795	13
7	1800	338	5933	18	1887	6	3702	11	3621	11	3506	10
8	4100	469	12755	27	4280	9	8030	17	7571	16	7233	15
9	3050	416	10008	24	3163	8	6070	15	5873	14	5609	13
10	2400	378	7650	20	2509	7	4804	13	4622	12	4476	12
11	2100	316	6925	22	2196	7	4320	14	4137	13	3995	13
12	4100	591	12755	22	4280	7	8030	14	7571	13	7233	12
13	4100	400	12755	32	4280	11	8030	20	7571	19	7233	18
14	4100	583	12755	22	4280	7	8030	14	7571	13	7233	12
15	4200	562	13275	24	4372	8	8163	15	7508	13	7377	13
16	1150	270	4026	15	1273	5	2459	9	2447	9	2351	9
17	1150	166	4026	24	1273	8	2459	15	2447	15	2351	14
18	1500	241	5070	21	1615	7	3118	13	3110	13	2960	12
19	5000	559	15820	28	5153	9	9608	17	9186	16	8602	15
Average		447	10157	22	3331	7	6289	14	6009	13	5739	13

Table 12 Ultimate axial load values of 300 mm wall thicknesses for 3DPC wall types in plan-2

Wall type			Filled		Carved		Square		Rectangular		Triangular	
No	L_w (mm)	Demand. axial load (kN)	Ulti. axial load (kN)	SF	Ulti. axial load (kN)	SF	Ulti. axial load (kN)	SF	Ulti. axial load (kN)	SF	Ulti. axial load (kN)	SF
1	5050	1128	31226	28	5460	5	10426	9	12829	11	9929	9
2	3650	667	22724	34	4065	6	7779	12	9583	14	7572	11
3	2100	480	14487	30	2455	5	4728	10	5847	12	4602	10
4	1800	545	12324	23	2088	4	3997	7	5028	9	4019	7
5	4100	782	25094	32	4482	6	8614	11	10511	13	8245	11
6	5050	910	31226	34	5460	6	10426	11	12829	14	9929	11
7	1800	490	12324	25	2088	4	3997	8	5028	10	4019	8
8	4100	717	25094	35	4482	6	8614	12	10511	15	8245	11
9	3050	602	19072	32	3398	6	6532	11	8160	14	6436	11
10	2400	545	15868	29	2767	5	5286	10	6429	12	5218	10
11	2100	458	14487	32	2455	5	4728	10	5847	13	4602	10
12	4100	810	25094	31	4482	6	8614	11	10511	13	8245	10
13	4100	576	25094	44	4482	8	8614	15	10511	18	8245	14
14	4100	851	25094	29	4482	5	8614	10	10511	12	8245	10
15	4200	802	25954	32	4558	6	8722	11	10360	13	8373	10
16	1150	367	8490	23	1412	4	2707	7	3258	9	2790	8
17	1150	244	8490	35	1412	6	2707	11	3258	13	2790	11
18	1500	345	10647	31	1774	5	3404	10	4323	13	3439	10
19	5000	825	30785	37	5393	7	10302	12	12705	15	9904	12
Average		639	20188	31	3536	5	6780	10	8318	13	6571	10

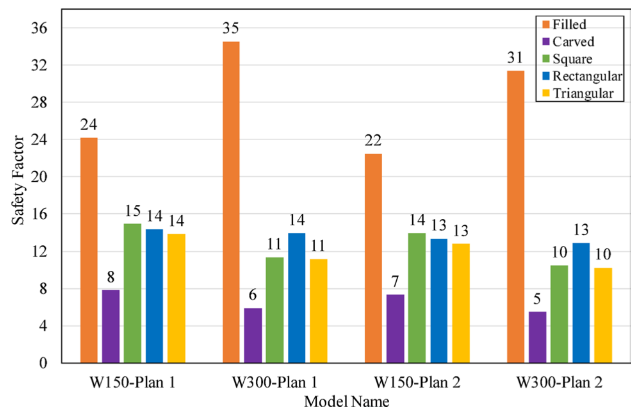

Fig. 9 Comparison of the average SF for all 3DPC wall types by wall thickness with the plan number

- The conclusions indicate the comparative ranking of wall types in the investigated high seismic demand scenario. Although an optimal configuration may vary based on location-specific seismic demands, wind dominance or site conditions, the comparative trends are applicable for a preliminary design option.

This study highlights that maximizing structural strength is not always the most effective strategy for 3D-printed buildings. While solid sections provide the highest load-bearing capacity, they come with excessive environmental and economic costs. Instead, the 'Carved' geometry offers a more practical balance, ensuring sufficient axial safety while significantly lowering carbon emissions and expenses. These findings suggest that design optimization should go beyond simple mechanics to include lifecycle considerations. Moving forward, experimental validation of shear and bending behaviors under cyclic loading will be crucial for integrating these geometries into seismic design codes.

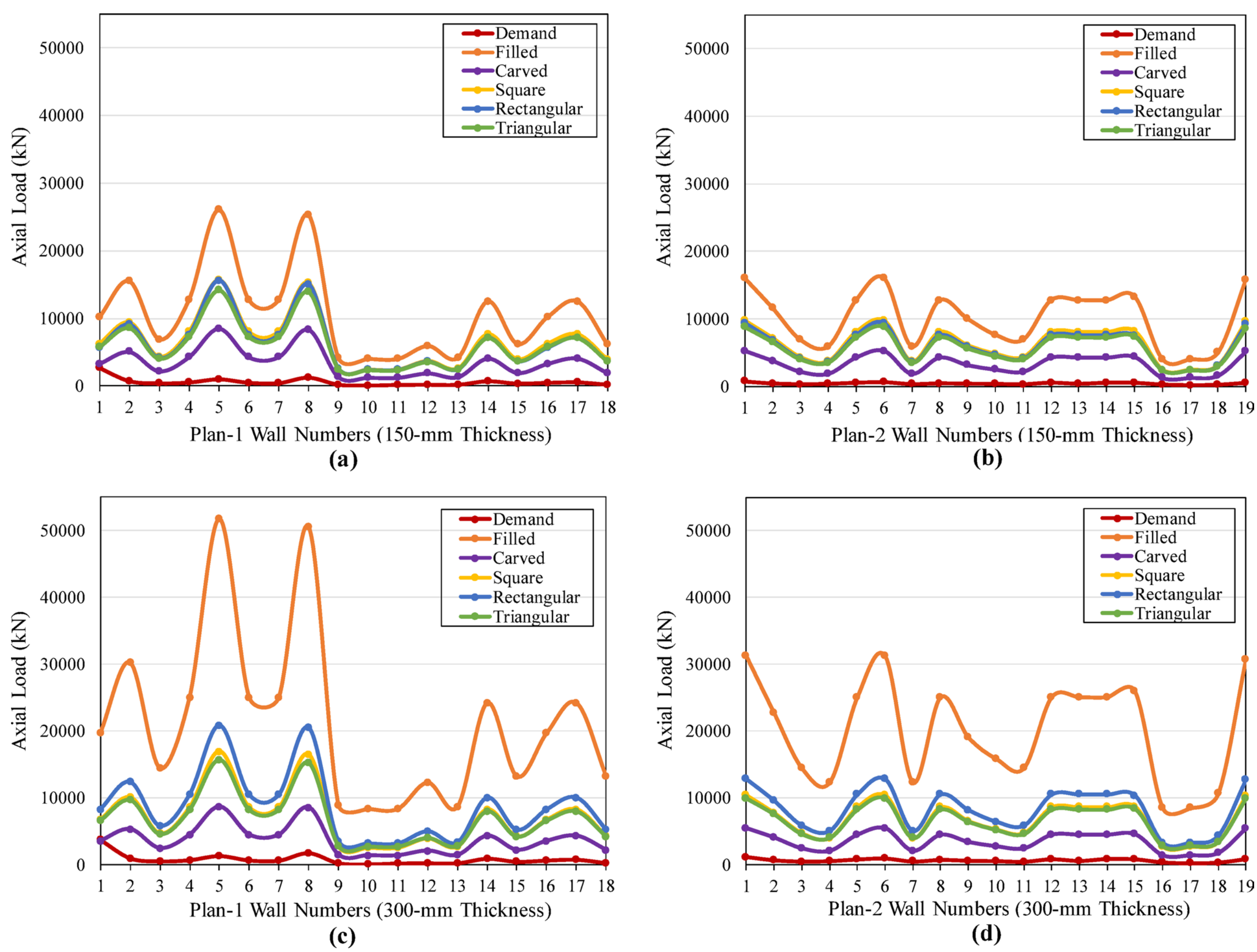

Fig. 10 Comparison of the ultimate axial load of each 3DPC wall according to wall type. **a** W150 in plan-1, **b** W150 in plan-2, **c** W300 in plan-1, **d** W300 in plan-2

Acknowledgements This publication is a part of doctoral dissertation work by the first author in the Academic Program of Civil Engineering, Institute of Science, Hacettepe University.

Author contributions İffet Gamze Mütevelli Özkan contributed to data curation, methodology, formal analysis, investigation, visualization, and writing - original draft preparation. Alper Aldemir contributed to methodology, supervision, conceptualization, and writing - review and editing.

Funding No funds, grants, or other support was received.

Data availability Data will be made available on reasonable request to the corresponding author.

Declarations

Conflict of interest The authors have no relevant financial or non-financial interests to disclose.

References

1. Craveiro F, Duarte JP, Bartolo H, Bartolo PJ (2019) Additive manufacturing as an enabling technology for digital construction: A perspective on Construction 4.0. Autom Constr 103:251–267. https://doi.org/10.1016/j.autcon.2019.03.011
2. Fernandez LIC, Caldas LR, Reales OAM (2023) Environmental evaluation of 3D printed concrete walls considering the life cycle perspective in the context of social housing. J Building Eng 74:106915. https://doi.org/10.1016/j.jobe.2023.106915
3. Olsson NO, Arica E, Woods R, Madrid JA (2021) Industry 4.0 in a project context: Introducing 3D printing in construction projects. Project Leadersh Soc 2:100033. https://doi.org/10.1016/j.plas.2021.100033
4. Burton M, Näsén K (2022) Simulation of load capacity of 3D printed concrete patterns
5. Agustí-Juan I, Habert G (2017) Environmental design guidelines for digital fabrication. J Clean Prod 142:2780–2791. https://doi.org/10.1016/j.jclepro.2016.10.190
6. Abdalla H, Fattah KP, Abdallah M, Tamimi AK (2021) Environmental footprint and economics of a full-scale 3D-printed house. Sustainability 13:11978. https://doi.org/10.3390/su132111978
7. Panda B, Tay YWD, Paul SC, Tan MJ (2018) Current challenges and future potential of 3D concrete printing: Aktuelle Herausforderungen und Zukunftspotenziale des 3D-Druckens bei Beton. Materialwissenschaft Werkst 49:666–673. https://doi.org/10.1002/mawe.201700279
8. Khan SA, Jassim M, Ilcan H et al (2023) 3D printing of circular materials: Comparative environmental analysis of materials and construction techniques. Case Stud Constr Mater 18:e02059. https://doi.org/10.1016/j.cscm.2023.e02059
9. Muñoz I, Alonso-Madrid J, Menéndez-Muñiz M et al (2021) Life cycle assessment of integrated additive–subtractive concrete 3D printing. Int J Adv Manuf Technol 112:2149–2159. https://doi.org/10.1007/s00170-020-06487-0
10. Dixit MK (2019) 3-D printing in building construction: a literature review of opportunities and challenges of reducing life cycle energy and carbon of buildings. In: IOP Conference Series: Earth and Environmental Science. IOP Publishing, p 012012 https://doi.org/10.1088/1755-1315/290/1/012012
11. De Schutter G, Lesage K, Mechtcherine V et al (2018) Vision of 3D printing with concrete—Technical, economic and environmental potentials. Cem Concr Res 112:25–36. https://doi.org/10.1016/j.cemconres.2018.06.001
12. Roux C, Kuzmenko K, Roussel N et al (2023) Life cycle assessment of a concrete 3D printing process. Int J Life Cycle Assess 28:1–15. https://doi.org/10.1007/s11367-022-02111-3
13. Gan VJ, Wong CL, Tse KT et al (2019) Parametric modelling and evolutionary optimization for cost-optimal and low-carbon design of high-rise reinforced concrete buildings. Adv Eng Inform 42:100962. https://doi.org/10.1016/j.aei.2019.100962
14. Agustí-Juan I, Müller F, Hack N et al (2017) Potential benefits of digital fabrication for complex structures: Environmental assessment of a robotically fabricated concrete wall. J Clean Prod 154:330–340. https://doi.org/10.1016/j.jclepro.2017.04.002
15. Tari MK, Faraji AR, Aslani A, Zahedi R (2023) Energy simulation and life cycle assessment of a 3D printable building. Clean Mater 7:100168. https://doi.org/10.1016/j.clema.2023.100168
16. Sakin M, Kiroglu YC (2017) 3D Printing of Buildings: Construction of the Sustainable Houses of the Future by BIM. Energy Procedia 134:702–711. https://doi.org/10.1016/j.egypro.2017.09.562
17. Comminal R, da Silva WRL, Andersen TJ et al (2020) Modelling of 3D concrete printing based on computational fluid dynamics. Cem Concr Res 138:106256. https://doi.org/10.1016/j.cemconres.2020.106256
18. Delavar MA, Chen H, Sideris P (2023) Seismic Design Methodology for 3D Printed Concrete Buildings. Cityscape 25:177–197. https://www.jstor.org/stable/48725039
19. Habert G, De Lacaillerie JD, Roussel N (2011) An environmental evaluation of geopolymer based concrete production: reviewing current research trends. J Clean Prod 19:1229–1238. https://doi.org/10.1016/j.jclepro.2011.03.012
20. Flower DJM, Sanjayan JG (2007) Green house gas emissions due to concrete manufacture. Int J Life Cycle Assess 12:282–288. https://doi.org/10.1065/lca2007.05.327
21. Chen C, Habert G, Bouzidi Y, Jullien A (2010) Environmental impact of cement production: detail of the different processes and cement plant variability evaluation. J Clean Prod 18:478–485. https://doi.org/10.1016/j.jclepro.2009.12.014
22. Eberhardt LCM, Van Stijn A, Rasmussen FN et al (2020) Towards circular life cycle assessment for the built environment: a comparison of allocation approaches. In: IOP Conference Series: Earth and Environmental Science. IOP Publishing, p 032026. https://doi.org/10.1088/1755-1315/588/3/032026
23. Gislason S, Bruhn S, Breseghello L et al (2022) Porous 3D printed concrete beams show an environmental promise: a cradle-to-grave comparative life cycle assessment. Clean Technol Environ Policy 24:2639–2654. https://doi.org/10.1007/s10098-022-02343-9
24. Yao Y, Hu M, Di Maio F, Cucurachi S (2020) Life cycle assessment of 3D printing geo-polymer concrete: An ex-ante study. J Industrial Ecol 24:116–127. https://doi.org/10.1111/jiec.12930
25. Motalebi A, Khondoker MAH, Kabir G (2024) A systematic review of life cycle assessments of 3D concrete printing. Sustainable Oper Computers 5:41–50. https://doi.org/10.1016/j.susoc.2023.08.003
26. Liu S, Lu B, Li H et al (2022) A comparative study on environmental performance of 3D printing and conventional casting of concrete products with industrial wastes. Chemosphere 298:134310. https://doi.org/10.1016/j.chemosphere.2022.134310
27. Weng Y, Li M, Ruan S et al (2020) Comparative economic, environmental and productivity assessment of a concrete bathroom unit fabricated through 3D printing and a precast approach. J Clean Prod 261:121245. https://doi.org/10.1016/j.jclepro.2020.121245
28. Zhang R-C, Wang L, Xue X, Ma G-W (2023) Environmental profile of 3D concrete printing technology in desert areas via life

cycle assessment. J Clean Prod 396:136412. https://doi.org/10.1016/j.jclepro.2023.136412
29. Mohammad M, Masad E, Al-Ghamdi SG (2020) 3D concrete printing sustainability: a comparative life cycle assessment of four construction method scenarios. Buildings 10:245. https://doi.org/10.3390/buildings10120245
30. Mishra SK, Snehal K, Das BB et al (2025) From printing to performance: a review on 3D concrete printing processes, materials, and life cycle assessment. J Building Pathol Rehabilitation 10:117. https://doi.org/10.1007/s41024-025-00626-4
31. Song J, Cao M, Cai L et al (2021) 3D printed polymeric formwork for lattice cementitious composites. J Building Eng 43:103074. https://doi.org/10.1016/j.jobe.2021.103074
32. Suntharalingam T, Upasiri I, Gatheeshgar P et al (2021) Energy performance of 3d-printed concrete walls: A numerical study. Buildings 11:432. https://doi.org/10.3390/buildings11100432
33. AlZahrani AA, Alghamdi AA, Basalah AA (2022) Computational Optimization of 3D-Printed Concrete Walls for Improved Building Thermal Performance. Buildings 12:2267. https://doi.org/10.3390/buildings12122267
34. Wolfs RJM, Bos FP, Salet TAM (2019) Hardened properties of 3D printed concrete: The influence of process parameters on interlayer adhesion. Cem Concr Res 119:132–140. https://doi.org/10.1016/j.cemconres.2019.02.017
35. Avrutis D, Nazari A, Sanjayan JG (2019) Industrial adoption of 3D concrete printing in the Australian market: potentials and challenges. 3D concrete Print Technol. https://doi.org/10.1016/B978-0-12-815481-6.00019-1
36. Lyu F, Zhao D, Hou X et al (2021) Overview of the development of 3D-printing concrete: A review. Appl Sci 11:9822. https://doi.org/10.3390/app11219822
37. Khan SA, Koç M, Al-Ghamdi SG (2021) Sustainability assessment, potentials and challenges of 3D printed concrete structures: A systematic review for built environmental applications. J Clean Prod 303:127027. https://doi.org/10.1016/j.jclepro.2021.127027
38. Roussel N (2018) Rheological requirements for printable concretes. Cem Concr Res 112:76–85. https://doi.org/10.1016/j.cemconres.2018.04.005
39. Mitrović SŽ, Ignjatović I (2024) Experimental investigation of bearing capacity of 3D printed concrete segmental girder. Building Mater Struct. https://doi.org/10.5937/GRMK2400008M
40. Figueiredo SC, Overmeir ALV, Nefs K et al (2020) Quality assessment of printable strain hardening cementitious composites manufactured in two different printing facilities. In: Bos FP, Lucas SS, Wolfs RJM, Salet TAM (eds) Second RILEM International Conference on Concrete and Digital Fabrication. Springer International Publishing, Cham, pp 824–838. https://doi.org/10.1007/978-3-030-49916-7_81
41. Mechtcherine V, Van Tittelboom K, Kazemian A et al (2022) A roadmap for quality control of hardening and hardened printed concrete. Cem Concr Res 157:106800. https://doi.org/10.1016/j.cemconres.2022.106800
42. Narjabadifam P, Mollaei S, Noroozinejad FE, Talebi SY (2024) Numerical analysis of seismic behavior of an arched-roof 3D-Printed building. Gra\djevinski materijali i konstrukcije 67:1–15. https://doi.org/10.5937/GRMK2300014P
43. Caron J-F, Demont L, Ducoulombier N, Mesnil R (2021) 3D printing of mortar with continuous fibres: Principle, properties and potential for application. Autom Constr 129:103806. https://doi.org/10.1016/j.autcon.2021.103806
44. Han X, Yan J, Liu M et al (2022) Experimental study on large-scale 3D printed concrete walls under axial compression. Autom Constr 133:103993. https://doi.org/10.1016/j.autcon.2021.103993
45. Jiramarootapong P, Prasittisopin L, Snguanyat C et al (2020) Load carrying capacity and failure mode of 3D printing mortar wall panel under axial compression loading. In: Second RILEM International Conference on Concrete and Digital Fabrication: Digital Concrete 2020 2. Springer, pp 646–657. https://doi.org/10.1007/978-3-030-49916-7_65
46. Daungwilailuk T, Pheinsusom P, Pansuk W (2021) Uniaxial load testing of large-scale 3D-printed concrete wall and finite-element model analysis. Constr Build Mater 275:122039. https://doi.org/10.1016/j.conbuildmat.2020.122039
47. Paudel S (2023) Investigation of modelling approaches to study the structural performance of 3D printed plain wall under uniform axial compression. Adv Struct Eng. https://doi.org/10.1177/13694332231166566
48. Özkan İGM, Aldemir A (2024) Machine-learning networks to predict the ultimate axial load and displacement capacity of 3D printed concrete walls with different section geometries. Struct Elsevier 106879. https://doi.org/10.1016/j.istruc.2024.106879
49. SAP2000 (2021) CSI Analysis Reference Manual for SAP2000, ETABS, SAFE and CSiBridge
50. TBEC 2018 (2018) Turkish Building Earthquake Code. Disaster and Emergency Management Presidency
51. Pırtı A (2023) Investigation the effects of earthquake in Golcuk-Izmit (17 Aug 1999) by using GPS. Arab J Geosci 16:646. https://doi.org/10.1007/s12517-023-11764-9
52. Öztürk H, Koral H, Geist EL (2000) Intra-basinal water movements induced by faulting: The August 17, 1999, Gölcük (İzmit Bay) earthquake (Mw = 7.4). Mar Geol 170:263–270. https://doi.org/10.1016/S0025-3227(00)00090-6
53. Efe R (2014) Earthquake Hazard Assessment in Turkey: the mw = 7.4, Gölcük (August 17, 1999) and the mw = 7.1, Düzce (November 12, 1999) earthquakes. Procedia-Social Behav Sci 120:629–636. https://doi.org/10.1016/j.sbspro.2014.02.143
54. TS 500 (2000) Requirements for Design and Construction of Reinforced Concrete Structures. Turkish Standards Institute
55. Álvarez-Fernández M-I, Prendes-Gero M-B, González-Nicieza C et al (2021) Optimum mix design for 3d concrete printing using mining tailings: A case study in Spain. Sustainability 13:1568. https://doi.org/10.3390/su13031568
56. BOLHASSANI D, YAVARTANOO F, TAPIA J et al (2024) The effect of post-tensioning on the behavior of small-scale 3D-printed concrete beams. In: Proceedings
57. Ji G, Ding T, Xiao J et al (2019) A 3D printed ready-mixed concrete power distribution substation: Materials and construction technology. Materials 12:1540. https://doi.org/10.3390/ma12091540
58. Alhumayani H, Gomaa M, Soebarto V, Jabi W (2020) Environmental assessment of large-scale 3D printing in construction: A comparative study between cob and concrete. J Clean Prod 270:122463. https://doi.org/10.1016/j.jclepro.2020.122463
59. Swamy RN (1998) Designing concrete and concrete structures for sustainable development. In: Sustainable Development of the Cement and Concrete Industry. Proceedings of CANMET/ACI International Symposium, Ottawa, Canada. pp 245–255
60. Akduman S, Aktepe R, Aldemir A et al (2024) Opportunities and challenges in constructing a demountable precast building using C&D waste-based geopolymer concrete: A case study in Türkiye. J Clean Prod 434:139976. https://doi.org/10.1016/j.jclepro.2023.139976
61. Elchalakani M, Aly T, Abu-Aisheh E (2014) Sustainable concrete with high volume GGBFS to build Masdar City in the UAE. Case Stud Constr Mater 1:10–24. https://doi.org/10.1016/j.cscm.2013.11.001
62. The Property Tribune (2023) How much does concrete cost per m3 in 2023. The Property Tribune. https://thepropertytribune.com.au/guides/building/how-much-does-concrete-cost-per-m3-in-2022/ Accessed 15 January 2026

63. Jeffery J (2025) How much does concreting cost? 2025 cost guide. Service.com.au. https://www.service.com.au/articles/concreters/how-much-does-concreting-cost Accessed 15 January 2026
64. Barcelo L, Kline J, Walenta G, Gartner E (2014) Cement and carbon emissions. Mater Struct 47:1055–1065. https://doi.org/10.1617/s11527-013-0114-5
65. Ozcelikci E, Kul A, Gunal MF et al (2023) A comprehensive study on the compressive strength, durability-related parameters and microstructure of geopolymer mortars based on mixed construction and demolition waste. J Clean Prod 396:136522. https://doi.org/10.1016/j.jclepro.2023.136522
66. Nisbet MA, VanGeem MG, Gajda J, Marceau M (2000) Environmental life cycle inventory of portland cement concrete. PCA R&D. Serial 28
67. Jones R, McCarthy M, Newlands M (2011) Fly ash route to low embodied CO2 and implications for concrete construction. In: World of Coal Ash (WOCA) Conference. pp 1–14